RSC Applied Interfaces

ROYAL SOCIETY OF CHEMISTRY

PAPER

View Article Online
View Journal | View Issue

Cite this: *RSC Appl. Interfaces*, 2025, **2**, 1821

Dual modification of $LiNbO_3$ and a lithium-conducting organic polymer at $LiCoO_2$/$Li_{10}GeP_2S_{12}$ interface and lithium intercalation properties in all-solid-state lithium-ion batteries

Kenta Watanabe, [a] Han-Seul Kim,[b] Yohei Hasegawa,[c] Steven W. Thompson, [d] Thiago R. Guimarães, [e] Ryoji Kanno, [c] Per B. Zetterlund *[d] and Masaaki Hirayama *[ac]

A lithium-conducting organic copolymer mainly comprising the comonomers poly(ethylene glycol) methyl ether methacrylate and lithium 3-[(trifluoromethane)sulfonamidosulfonyl]propyl methacrylate (LiMTFSI) (referred to as "Li-polymer") was coated on $LiNbO_3$-modified $LiCoO_2$ particles. The *in situ* polymerization was conducted *via* reversible addition–fragmentation chain transfer (RAFT) assisted encapsulating polymerisation (REEP) to form the Li-polymer coating, aiming to enhance the electrochemical stability of cathode-sulfide electrolyte interfaces in all-solid-state lithium-ion batteries. The formation of a thin Li-polymer layer on the $LiNbO_3$/$LiCoO_2$ surface was confirmed through X-ray diffraction, scanning electron microscopy with energy-dispersive X-ray spectroscopy, and thermogravimetric analysis. These analyses indicated no structural changes of $LiNbO_3$-modified $LiCoO_2$ during the modification process with Li-polymer. Galvanostatic charge–discharge and electrochemical impedance spectroscopy analyses revealed that, among the Li-polymer/$LiNbO_3$/$LiCoO_2$–$Li_{10}GeP_2S_{12}$ composite cathodes, the composite incorporating a Li-polymer containing 50% LiMTFSI, with a higher lithium content and low glass-forming tendency, demonstrated the highest electrochemical activity. However, even with 50% LiMTFSI-containing Li-polymer, the capacity remained lower than that of $LiNbO_3$/$LiCoO_2$–$Li_{10}GeP_2S_{12}$. On the other hand, under high-voltage charging, the Li-polymer–coated composite demonstrated improved capacity retention compared to the Li-polymer–uncoated composite. These findings highlight the potential of organic polymer modification layers to enhance the interfacial stability of high-voltage all-solid-state lithium-ion batteries (ASBs) with sulfide solid electrolytes.

Received 23rd July 2025,
Accepted 8th September 2025

DOI: 10.1039/d5lf00209e

rsc.li/RSCApplInter

Introduction

All-solid-state lithium-ion batteries (ASBs) with sulfide solid electrolytes have attracted significant attention as power sources for large-scale applications owing to their inherently high energy density, high power characteristics, and high reliability.[1–9] However, the degradation of ionic conductivity between the active material and solid electrolyte in composite electrodes occurs,[7,10–15] specifically for high-voltage ASBs. This degradation is attributed to (i) the formation of a highly resistive interlayer through side reactions at interfaces[7,10,11] and (ii) the loss of sufficient interfacial contact for ionic and electronic conduction owing to the volumetric changes in the active materials.[12–15] Surface modification of lithium-containing inorganic oxides, such as $LiNbO_3$ (ref. 16) and $Li_4Ti_5O_{12}$,[17] has been proven to suppress the formation of a highly resistive interlayer by preventing direct contact between the active material and the solid electrolyte. However, since these modification layers are as rigid as the active materials and solid electrolytes, mechanical failures such as interfacial separation and cracking induced by volumetric changes still persist. Modification materials that can relieve the mechanical stress are highly desired to ensure sufficient contact area and ion conduction pathways. To further enhance physical

[a] *Department of Chemical Science and Engineering, School of Materials and Chemical Technology, Institute of Science Tokyo, Yokohama 226-8501, Japan. E-mail: hirayama@mct.isct.ac.jp*
[b] *Department of Chemical Science and Engineering, School of Materials and Chemical Technology, Tokyo Institute of Technology, Yokohama 226-8501, Japan*
[c] *Research Center for All-Solid-State Battery, Institute of Integrated Research, Institute of Science Tokyo, Yokohama 226-8501, Japan*
[d] *Cluster for Advanced Macromolecular Design (CAMD), School of Chemical Engineering, University of New South Wales, Sydney, NSW 2052, Australia. E-mail: p.zetterlund@unsw.edu.au*
[e] *Laboratoire de Chimie des Polymères Organiques (LCPO, UMR5629), CNRS, Bordeaux INP, University of Bordeaux, F-33607 Pessac, France*

stability, the present study applies an organic polymer coating as a secondary modification layer over the inorganic oxide coating. Organic materials typically exhibit softer characteristics than inorganic oxides.[18–20] Polymer coatings have demonstrated positive effects on cathode materials in liquid-type lithium-ion batteries by buffering volume changes and suppressing particle cracking.[21–25] In recent years, several studies have reported the incorporation or impregnation of polymer materials into electrode composites for oxide-type solid-state batteries to improve electronic conductivity and mechanical strength.[19,20,26–29] However, there have been few reports on the modification of organic polymers between electrodes and sulfide electrolyte interfaces.[30,31] Poly(ethylene glycol) methyl ether methacrylate (PEGMA) is a soft hydrophilic monomer with a low glass-transition temperature.[32–34] Surface modification of PEGMA on electrode particles is expected to relieve the stress induced by volumetric changes, leading to improved retention of inter-grain connections.[35] Because PEGMA does not exhibit lithium-ion conductivity, in the present study it was copolymerised with a lithium-conducting monomer. Recently, we succeeded in polymerising PEGMA with lithium 3-[(trifluoromethane) sulfonamidosulfonyl]propyl methacrylate (LiMTFSI) on the surface of $LiNbO_3$-coated $LiCoO_2$ particles *via* reversible addition–fragmentation chain transfer (RAFT) assisted encapsulating polymerisation (REEP).[36] REEP is a two-step process whereby a macroRAFT agent is first adsorbed onto the inorganic particle surfaces, followed by a RAFT-mediated chain extension resulting in a polymer shell around the particles.[37] This process leverages RAFT polymerization, a controlled/living radical polymerization technique that enables precise control over polymer molecular weight, architecture, and block copolymer formation, even in heterogeneous systems.[38] REEP has been shown to be a powerful technique for the efficient encapsulation of inorganic materials such as metal oxides,[39–41] carbon nanotubes,[42] graphene oxide,[43] and layered double hydroxides.[44] The REEP process is beneficial as it allows for uniformity in coating thickness which can be tuned *via* monomer/inorganic material ratios,[37] the encapsulation of non-spherical particles, and directing the encapsulation towards the inorganic material rather than new particle formation in the aqueous phase.[45] Despite its limited application in battery research, REEP has been widely utilized in other fields, including catalysis,[46] drug delivery,[47] and colloidal stabilization,[45] due to its ability to provide conformal, uniform coatings on diverse inorganic substrates. In the present study, we fabricated cathode composites comprising Li-polymer-encapsulated $LiNbO_3/LiCoO_2$ and a $Li_{10}GeP_2S_{12}$ solid electrolyte, and characterised their electrochemical properties using ASBs using an In–Li anode. X-ray diffraction (XRD), scanning electron microscopy with energy-dispersive X-ray spectroscopy (SEM-EDX), and thermogravimetric (TG) analysis were used to verify the formation of a thin Li-polymer layer. The effects of the weight ratio of LiMTFSI to PEGMA on the charge–discharge activity were investigated to design facile ionic conduction at the cathode interface. The charge–discharge properties under high voltages were also investigated to compare the electrochemical stability of the unencapsulated $LiNbO_3/LiCoO_2$–$Li_{10}GeP_2S_{12}$ cathode composite.

Experimental

Commercialised $LiCoO_2$ powder (Nippon Chemical Industry; C-5H, average diameter: 7.96 μm) was used, and the $LiCoO_2$ surface was coated with amorphous $LiNbO_3$ through a spray coating method.[10,48] LiMTFSI/PEGMA/EGDMA (Li-polymer) was further coated onto the surface of $LiNbO_3$-coated $LiCoO_2$ particles *via* RAFT assisted encapsulating polymerisation (REEP).[36] The change in the crystal structure after the Li-polymer coating was investigated by XRD acquired at 298 K using an X-ray powder diffractometer (Rigaku; SmartLab) using Cu $K\alpha_1$ radiation over the 10–70° 2θ range in increments of 0.02°. TG curves were collected in Ar using a TG/differential thermal analyzer (Rigaku; Thermo plus TG8120). The temperature range was 298–773 K and heating and cooling rate was 10 K min^{-1}.

The $Li_{10}GeP_2S_{12}$ (LGPS) solid electrolyte and cathode composites of Li-polymer/$LiNbO_3/LiCoO_2$–LGPS were synthesised using a previously reported procedure.[48] SEM-EDX analysis was performed using a field-emission-SEM (Hitachi High-Tech; Regulus 8230) equipped with an EDX (Bruker; QUANTAX FlatQUAD). The Li-polymer/$LiNbO_3/LiCoO_2$–$Li_{10}GeP_2S_{12}$ was pelletised and cut using a multi-angle slicer (JASCO; Slice Master HW-1). The cross section of the cut pellet was flattened through ion milling (Hitachi High-Tech; IM4000 plus) at 183 K for 2 h using an Ar ion beam.[49,50] The SEM-EDX observations were conducted under an electron beam acceleration voltage of 5 kV and an emission current of 10 μA. EDX images were collected at an integration time of 120 s.

The charge and discharge characteristics of the cathode composites were investigated using two-electrode all-solid-state batteries of Li-polymer/$LiNbO_3/LiCoO_2$–LGPS/LGPS/In–Li to analyse the electrochemical properties of the composite electrodes.[48] Charge–discharge measurements were performed at 298 K using a multichannel potentiostat/galvanostat (Toyo system; TOSCAT-3100). The upper and lower cut-off voltages were 3.6–4.0 V and 1.9 V, respectively, under an applied current rate of 6.85 mA g^{-1} (0.05C for $LiCoO_2$). Specific capacities were calculated based on the active mass of Li-polymer/$LiNbO_3/LiCoO_2$. Constant-current/constant-voltage and constant-current modes were used for the charge and discharge measurements, respectively. The interfacial resistances at the electrode/electrolyte were measured using electrochemical impedance spectroscopy (EIS) (Solartron; 1260/1287). The impedance spectra were measured after charging at an applied alternating current (AC) voltage and frequency range of 10 mV and 10^6–10^{-2} Hz, respectively.

Results and discussion

Structural characterisation

We have previously carefully investigated RAFT assisted encapsulating polymerisation to encapsulate $LiNbO_3/LiCoO_2$ particles with lithium containing polymer (Scheme 1) – the synthesis of all the materials tested in the present work have been fully described in our previous paper.[36] The Li-polymer

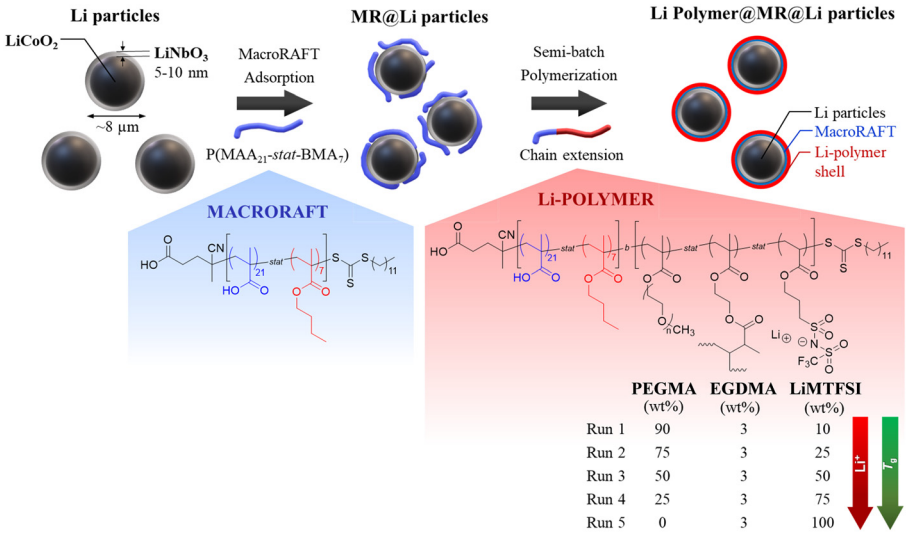

Scheme 1 RAFT assisted encapsulating polymerisation of $LiNbO_3/LiCoO_2$ with different LiMTFSI/PEGMA content.

layer is a diblock copolymer, with the first block consisting of an macroRAFT (Scheme 1) which provides adsorption to the surface of the $LiNbO_3/LiCoO_2$ particles and provides stability to the particles in water. The second block has varying weight fractions of PEGMA/LiMTFSI ranging from 90/10 PEGMA/LiMTFSI up till 0/100 LiMTFSI. The second blocks are all crosslinked with ethylene glycol dimethacrylate (EGDMA), 3 wt% relative to overall monomer mass, to enhance encapsulation of the $LiNbO_3/LiCoO_2$ particles. The $LiNbO_3$ layer was introduced as a protective interlayer aimed at suppressing the oxidative decomposition of the polymer caused at the $LiCoO_2$ surface.

In the present work, we have first examined the structural changes in the $LiNbO_3/LiCoO_2$ particles following RAFT assisted encapsulating polymerisation (REEP) using XRD, SEM-EDX, and TG measurements. Li-polymer/$LiNbO_3/LiCoO_2$ and the original $LiNbO_3/LiCoO_2$ exhibit diffraction peaks that can be indexed to layered rocksalt-type $LiCoO_2$ (Fig. 1a). The lattice parameters of a and c were calculated to be 2.8157(4) Å and 14.048(3) Å and 2.8165(5) Å and 14.053(3) Å for Li-polymer/$LiNbO_3/LiCoO_2$ and $LiNbO_3/LiCoO_2$, respectively. These results confirmed that no chemical reaction occurred between $LiCoO_2$, $LiNbO_3$, and the monomers/polymer during polymerisation in an aqueous medium and under vacuum drying at 323 K. SEM-EDX images show that Li-polymer/$LiNbO_3/LiCoO_2$ has a particle size similar to that of $LiCoO_2$ and a surface morphology similar to the that of the original $LiNbO_3/LiCoO_2$ (Fig. 1b), indicating the formation of a thin Li-polymer layer on the $LiNbO_3/LiCoO_2$ particle surfaces, with no significant degradation of the surface structure. TG curves in Fig. 1c show the weight losses of Li-polymer/$LiNbO_3/LiCoO_2$ and $LiNbO_3/LiCoO_2$ during the heating and cooling processes under oxygen. Both samples exhibited a weight loss of less than 0.4% up to 423 K, confirming the removal of residual water from the Li-polymer matrix during drying. Therefore, Li-polymer/$LiNbO_3/LiCoO_2$ is suitable for compositing with LGPS-type solid electrolytes that are unstable in moisture. However, above 423 K, Li-polymer/$LiNbO_3/LiCoO_2$ experienced greater weight loss than $LiNbO_3/LiCoO_2$, which was attributed to the decomposition of polymer. The difference in weight loss between the samples was only 2.5% at 773 K, further supporting the formation of

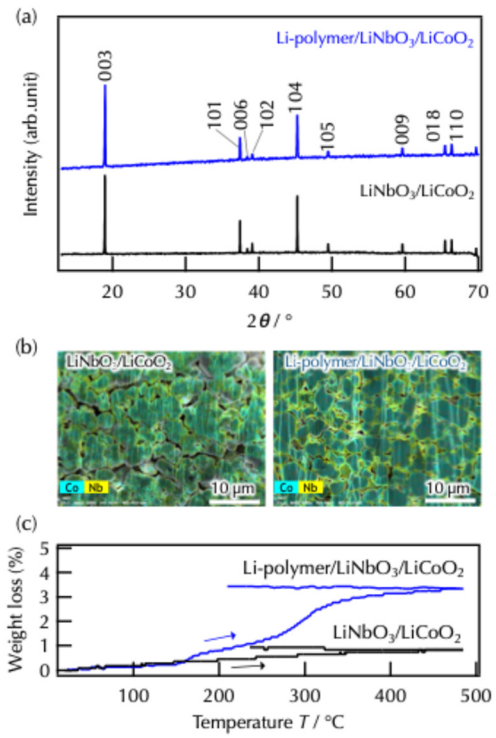

Fig. 1 (a) XRD patterns, (b) SEM-EDX images, and (c) TG curves of $LiNbO_3/LiCoO_2$ and Li-polymer/$LiNbO_3/LiCoO_2$. The Li-polymer/$LiNbO_3/LiCoO_2$ was dried in vacuum at 213 and 323 K. The weight ratio of lithium 3-[(trifluoromethane)sulfonamidosulfonyl]propyl methacrylate (LiMTFSI) to PEGMA was 50%.

a thin layer of Li-polymer on the $LiNbO_3/LiCoO_2$ particle surfaces.

Effects of LiMTFSI content on charge–discharge activity

Fig. 2a–e shows the charge–discharge curves for encapsulated $LiNbO_3/LiCoO_2$ cathodes at varying weight ratios of LiMTFSI to PEGMA. The charge current density was fixed at 0.05C, and the discharge current density was increased from 0.05 to 1C every three cycles. The discharge capacity retentions corresponding to different discharge C rates are shown in Fig. 2f. For the 10% and 25% LiMTFSI-containing Li-polymer samples, the cell voltage increased rapidly to a cut-off voltage of 3.6 V at the start of constant-current charging. The capacity gradually increased to approximately 65 mAh g^{-1} during constant-voltage charging, indicating a high overvoltage of electrochemical reaction. The discharge reaction occurred at approximately 3 V *vs.* In–Li, indicating lithium intercalation into the $LiCoO_2$ cathode.[48] However, the discharge capacity was approximately 60 mAh g^{-1} when discharged at 0.05C, which was significantly lower than that observed for a $LiNbO_3/LiCoO_2$–LGPS composite cathode (110 mAh g^{-1}).[48] In addition, the discharge capacities decreased significantly when discharged at 0.1 and 0.5C, suggesting the formation of insufficient conduction pathways for Li ions in the Li-polymer layer. In contrast, the 50% LiMTFSI-coated cathode exhibited an evident slope during constant-current charging, achieving a charge capacity of 90 mAh g^{-1} after constant-voltage charging. During discharge, the 50% LiMTFSI-coated cathode exhibited a higher discharge capacity of over 80 mAh g^{-1} at 0.05C, with higher discharge voltages than the 10% and 25% LiMTFSI-coated cathodes. Furthermore, lithium intercalation proceeded even at 1C operation. These results suggested that a higher LiMTFSI content improved Li conductivity in the polymer layer. Conversely, the 75% LiMTFSI-containing Li-polymer exhibited a reduced discharge of 60 mAh g^{-1} at 0.05C, although its discharge voltage was slightly higher than that of the 50% LiMTFSI-containing Li-polymer. The 100% LiMTFSI-containing Li-polymer exhibited a further decrease in the discharge capacity (40 mAh g^{-1}).

To further investigate the superior charge–discharge activity of Li-polymer-coated $LiNbO_3/LiCoO_2$ with moderate LiMTFSI content, EIS analyses were conducted for the cell after the cycle tests. Fig. 3a shows Nyquist plots for the Li-polymer/$LiNbO_3/LiCoO_2$–LGPS composite cathodes with different weight ratios of LiMTFSI to PEGMA. Magnified views of the high-frequency region are shown in Fig. 3b. Two semicircles were observed in all the samples, with the semicircles observed at higher frequencies exhibiting no significant changes with varying LiMTFSI content. In contrast, the semicircles observed at lower frequencies exhibited significant changes at varying LiMTFSI content, primarily attributed to variations in the resistive component within the cathode composites. The resistance (R), constant phase element (CPE), and Warburg impedance (W) values of

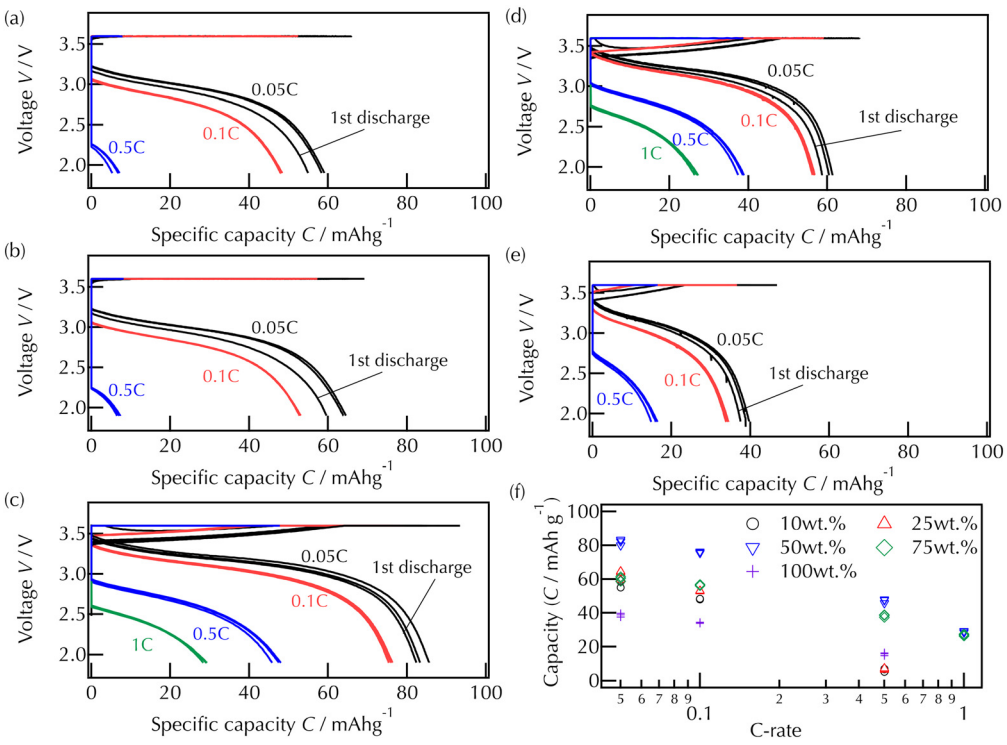

Fig. 2 Charge–discharge curves of Li-polymer/$LiNbO_3/LiCoO_2$–$Li_{10}GeP_2S_{12}$ (LGPS) composite cathodes with different weight ratios of LiMTFSI to PEGMA: (a) 10, (b) 25, (c) 50, (d) 75, and (e) 100 wt%. (f) Variations in the discharge capacity retention with different C rates. All tests were conducted at 298 K (25 °C). The discharge current density increased from 0.05 and 1C every three cycles.

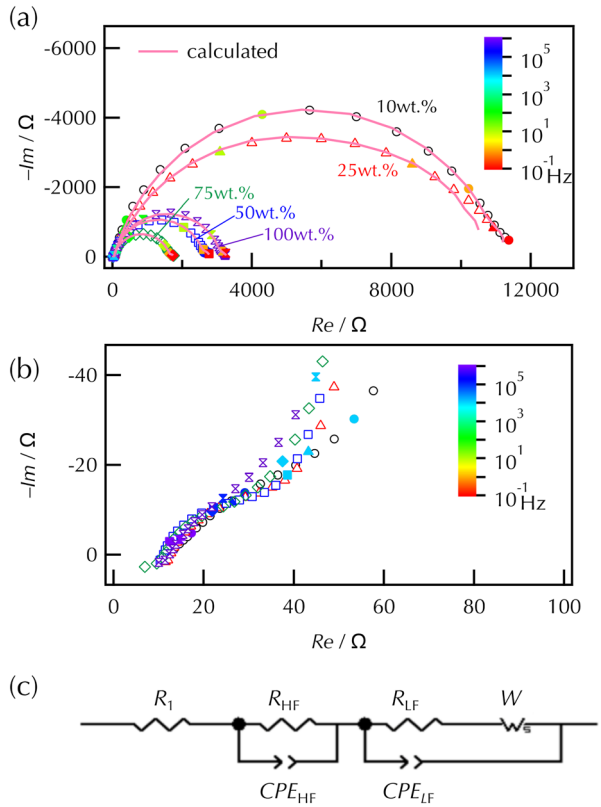

Fig. 3 (a) Nyquist plots and fitting curves of all-solid-state batteries using Li-polymer/$LiNbO_3$/$LiCoO_2$–LGPS composite cathodes at varying weight ratios of LiMTFSI to PEGMA of 10, 25, 50, 75, and 100 wt%. EIS data were collected after the cycle tests. (b) Enlarged spectra of (a) high-frequency region. (c) Equivalent circuit model used for curve-fitting.

each component were refined by fitting the equivalent circuit models, as shown in Fig. 3c. The fitted curves are shown in Fig. 3a, and the refined R and capacitance (C) parameters are summarised in Table 1. The C values were calculated using R and CPE values. All batteries exhibited C_{LF} values of the order of 10^{-6} F, aligning with the reported charge transfer resistances at the $LiNbO_3$/$LiCoO_2$–LGPS interface (1.1×10^{-6} F).[48] This result indicated that the semicircles observed at lower frequencies corresponded to the interfacial resistance between the Li-polymer/$LiNbO_3$/$LiCoO_2$ cathode and the LGPS electrolyte. The 10% and 25% PLiMTFSI-containing Li-polymer-coated cathodes exhibit high R_{LF} values of over 10^4 Ω, which are consistent with the high overvoltage observed in the charge–discharge curves (Fig. 2a and b). The R_{LF} value decreases to 2.5×10^3 Ω for the 50% LiMTFSI-containing Li-polymer, correlating with improved intercalation properties (Fig. 2c). The R_{LF} value further decreases to 1.6×10^3 Ω for the 75% LiMTFSI-containing Li-polymer, which is consistent with the high discharge voltages observed in the discharge curves (Fig. 2d) compared to that of the 50% LiMTFSI-containing Li-polymer (Fig. 2c). Generally, the interfacial resistance (R_{LF}) depends on the resistivity of lithium intercalation and the interfacial area. Considering that there were no significant differences in the $LiCoO_2$ and LGPS particles among the samples, a high LiMTFSI content enhanced the lithium conductivity in the polymer layer, facilitating faster lithium intercalation at the cathode interface. The 100% LiMTFSI-containing Li-polymer-coated sample exhibited an increase in R_{LF} value (3.1×10^3 Ω). Although a higher amount of lithium monomer/polymer would be expected to be beneficial for battery charge capacity, an increase in glass transition temperature (T_g) has been shown to lead to a decrease in ionic conductivity due to low lithium-ion mobility in the glassy phase.[32] The theoretical T_g values assuming no crosslinker are 267, 307, and 368 K for 50, 75, and 100 wt% LiMTFSI.[36] As a result at 298 K, for the 75% and 100% LiMTFSI-containing Li-polymer, the polymer would be in a glassy state. This finding explains the decrease in the charge–discharge capacities observed for the 75% and 100% LiMTFSI-containing Li-polymer-coated cathodes.

The small charge–discharge capacities of Li-polymer/$LiNbO_3$/$LiCoO_2$ compared to $LiNbO_3$/$LiCoO_2$ without an organic coating may be primarily attributed to the poor ionic conductivity of the Li-polymer layer. To verify this result, charge–discharge measurements were conducted at 333 K to enhance ionic conductivity. Fig. 4 shows the charge–discharge curves for the 25% Li-polymer/$LiNbO_3$/$LiCoO_2$–LGPS cathode composite at 333 K. For comparison, the charge–discharge curves of a $LiNbO_3$/$LiCoO_2$–LGPS cathode composite at 298 K are also shown. The 25% Li-polymer/

Table 1 Fitting results of EIS analyses for all-solid-state batteries using Li-polymer/$LiNbO_3$/$LiCoO_2$–$Li_{10}GeP_2S_{12}$ composite cathodes with weight ratios of lithium LiMTFSI to PEGMA of 10, 25, 50, 75, and 100 wt%

LiMTFSI content (wt%)	R_1/Ω	R_{HF}/Ω	C_{HF}/F	R_{LF}/Ω	C_{LF}/F
10	13.1	32.4	4.6×10^{-8}	1.1×10^4	2.2×10^{-6}
25	12.8	27.0	1.1×10^{-8}	1.0×10^4	4.1×10^{-6}
50	10.8	29.3	8.8×10^{-8}	2.5×10^3	2.6×10^{-6}
75	9.8	26.0	8.1×10^{-8}	1.6×10^3	2.0×10^{-6}
100	12.0	26.9	8.7×10^{-8}	3.1×10^3	1.8×10^{-6}

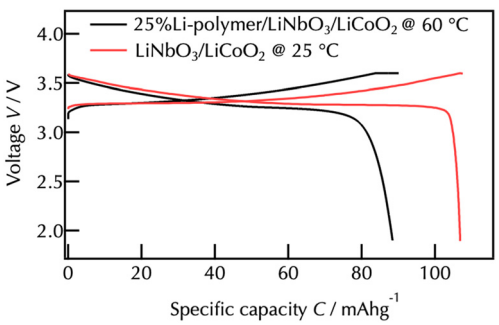

Fig. 4 Charge–discharge curves of 25% Li-polymer/$LiNbO_3$/$LiCoO_2$–LGPS at 333 K (60 °C) and $LiNbO_3$/$LiCoO_2$–LGPS at 298 K (25 °C). The charge–discharge current density is 0.05C. Charge–discharge curves of 25% Li-polymer/$LiNbO_3$/$LiCoO_2$–LGPS at 298 K is shown in Fig. 2b.

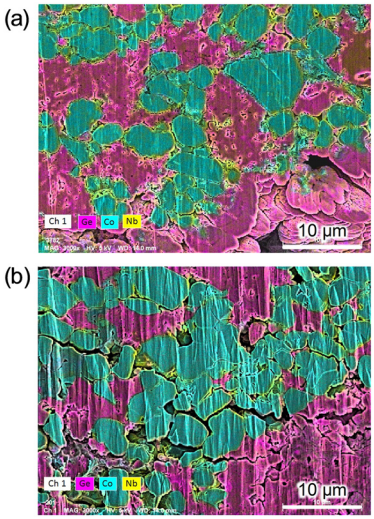

Fig. 5 SEM-EDX images of (a) 25% Li-polymer/$LiNbO_3$/$LiCoO_2$–LGPS and (b) $LiNbO_3$/$LiCoO_2$–LGPS cathode composites.

$LiNbO_3$/$LiCoO_2$ exhibited evident plateau regions in the charge and discharge curves and achieved high charge–discharge capacities of approximately 90 mAh g^{-1}. The average discharge voltage was approximately 3.26 V, which was comparable to that of $LiNbO_3$/$LiCoO_2$–LGPS (3.33 V). These results reveal a significant improvement in the lithium intercalation activity compared to that observed at 298 K (Fig. 2b). However, the charge–discharge capacities of Li-polymer/$LiNbO_3$/$LiCoO_2$ were lower than those of $LiNbO_3$/$LiCoO_2$. Fig. 5 shows the SEM-EDX images of the 25% Li-polymer/$LiNbO_3$/$LiCoO_2$–LGPS and $LiNbO_3$/$LiCoO_2$–LGPS cathode composites. In the 25% Li-polymer/$LiNbO_3$/$LiCoO_2$–LGPS composite, some $LiNbO_3$/$LiCoO_2$ particles were isolated. The Li-polymer-coated $LiNbO_3$/$LiCoO_2$ particles were less aggregated, resulting in a high dispersion with the LGPS particles. Consequently, the interfacial area between $LiNbO_3$/$LiCoO_2$ and LGPS increased, the electronic contact between the $LiNbO_3$/$LiCoO_2$ particles was disrupted, leading to low utilisation of the $LiCoO_2$ active material. In contrast, the $LiNbO_3$/$LiCoO_2$ particles in $LiNbO_3$/$LiCoO_2$–LGPS were in relatively good contact with each other, suggesting the establishment of electronic conduction pathways. Based on these results, the reduced charge–discharge capacities of Li-polymer/$LiNbO_3$/$LiCoO_2$ were associated with the poor ionic conductivity of the Li-polymer layer and inadequate electronic conduction pathways among the $LiNbO_3$/$LiCoO_2$ particles. We have previously reported that, in well-dispersed $LiNbO_3$/$LiCoO_2$–LGPS composites, there is a trade-off between the increased interfacial area and the decreased electronic conduction pathways, and that increasing the $LiNbO_3$/$LiCoO_2$-to-LGPS ratio is necessary to secure sufficient electronic conductivity.[51] Therefore, the charge and discharge capacities of Li-polymer/$LiNbO_3$/$LiCoO_2$ could be enhanced by improving electronic conductivities such as adjusting the $LiCoO_2$/LGPS ratio and introducing carbon additives.

Electrochemical stability at high voltage regions

Preliminary investigations were conducted to evaluate the electrochemical stability of the Li-polymer layer in high-voltage regions. Constant-voltage charging was conducted until the current density decayed to a pre-set value of 4 μA, ensuring high voltage conditions at the cathode interface. Fig. 6 shows the charge–discharge curves of the 50% Li-polymer/$LiNbO_3$/$LiCoO_2$–LGPS and $LiNbO_3$/$LiCoO_2$–LGPS composite cathodes in the voltage region of 4.0–1.9 V. In the first cycle, the Li-polymer/$LiNbO_3$/$LiCoO_2$ composite achieved charge and discharge capacities of 128 and 122 mAh g^{-1}, respectively, which exceeded those obtained with an upper cut-off voltage of 3.6 V (Fig. 2c). The additional plateau observed at approximately 3.4 V in the discharge curve indicates that further lithium (de)intercalation proceeded at high voltages. The initial coulombic efficiency was calculated to be 95.3%. The charge and discharge capacities were 114 and 113 mAh g^{-1} by the fifth cycle, respectively, despite a decrease in the discharge voltage. In contrast, $LiNbO_3$/$LiCoO_2$–LGPS achieved the first charge and discharge capacities of 175 and 146 mAh g^{-1}, respectively. The initial Coulombic efficiency was 83.4%, which was significantly lower than that of the Li-polymer/$LiNbO_3$/$LiCoO_2$–LGPS composite. Subsequently, the charge and discharge capacities significantly decreased to 111 and 106 mAh g^{-1} by the fifth cycle, falling below the corresponding values of Li-polymer/$LiNbO_3$/$LiCoO_2$. $LiCoO_2$ undergoes a similar degree of volume change during lithium (de)intercalation even when charged up to 4.0 V compared to 3.6 V,[52] indicating that the capacity fading is unlikely to originate from mechanical degradation of the cathode composite. The severe decrease in capacity could be associated with formation of a resistive interphase

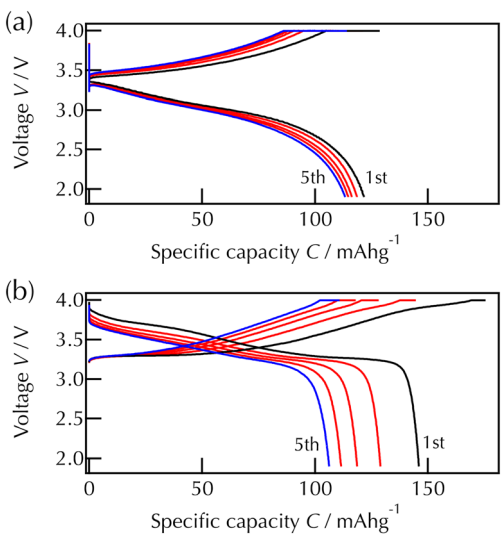

Fig. 6 Charge–discharge curves of (a) 50% Li-polymer/$LiNbO_3$/$LiCoO_2$–LGPS and (b) $LiNbO_3$/$LiCoO_2$–LGPS composite cathodes in the voltage region of 4.0–1.9 V. The charge–discharge tests are conducted at 298 K and 0.05C.

caused by irreversible side reactions at the $LiNbO_3$/sulfide electrolyte interface above 3.8 V (4.4 V *vs.* Li).[11] The relatively high cycle retention and Coulombic efficiency observed for the Li-polymer/$LiNbO_3$/$LiCoO_2$ composite suggests the following possible mechanisms: (i) the larger interfacial area between $LiNbO_3$/$LiCoO_2$ and LGPS, as shown in Fig. 5(a), results in only a modest increase in overall interfacial resistance, although interfacial side reactions increase the area-specific resistance. (ii) The Li-polymer layer is highly electrochemically stable at the interface with $LiNbO_3$ and LGPS, or (iii) the side reaction products generated at high voltages are electrochemically stable and ion conductive.[32] While further improvement in the utilization of $LiCoO_2$ within the Li-polymer/$LiNbO_3$/$LiCoO_2$ + LGPS composite and a more comprehensive investigation of its mechanical cycle stability based on microstructural evolution are required, we successfully demonstrated the high electrochemical stability of the polymer-modified cathode/sulfide electrolyte interface. This finding offers a new perspective for the development of highly functional electrode composites in sulfide-based ASBs.

Conclusions

A lithium-ion conducting polymer was coated onto the $LiNbO_3$/$LiCoO_2$ surface using RAFT assisted encapsulating polymerisation (REEP). A bulk-type all-solid-state battery utilising a Li-polymer/$LiNbO_3$/$LiCoO_2$ cathode composite, an LGPS electrolyte, and a Li anode demonstrated successful operation. The $LiNbO_3$/$LiCoO_2$ modified with a 50 wt% LiMTFSI-containing Li-polymer layer achieved the highest reversible lithium (de)intercalation with a discharge capacity of exceeding 80 mAh g^{-1} at 0.05C. EIS analyses revealed that LiMTFSI was effectively integrated into the PEGMA structure, creating lithium conduction pathways for lithium ions. However, the Li-polymer coated $LiCoO_2$ particles were highly dispersed within the LGPS matrix, leading to poor electronic conduction in the cathode composites and resulting in a decrease in utilization of the $LiCoO_2$ active material. At high voltages, Li-polymer/$LiNbO_3$/$LiCoO_2$ exhibited high cycle retention with a high Coulombic efficiency compared to $LiNbO_3$/$LiCoO_2$, owing to the high electrochemical stability of the Li-polymer layer. The lithium ion-conducting organic polymer can be a promising modification material to enhance the stability of oxide-cathode/sulfide-electrolyte interfaces in high-voltage ASBs.

Conflicts of interest

There are no conflicts to declare.

Data availability

The data that support the findings of this work are available within the article.

Acknowledgements

This study was partially supported by a Grant-in-Aid for Scientific Research on Innovative Areas (No. 19H05793) from the Japan Society for the Promotion of Science (JSPS) and Japan Science and Technology Agency (JST) as part of Adopting Sustainable Partnerships for Innovative Research Ecosystem (ASPIRE), JPMJAP2407. We thank Ms. Naomi Inazu of the Tokyo Institute of Technology for her kind assistance in SEM-EDX measurements.

References

1 J. Janek and W. G. Zeier, *Nat. Energy*, 2016, **1**, 16141.
2 S. P. Culver, R. Koerver, T. Krauskopf and W. G. Zeier, *Chem. Mater.*, 2018, **30**, 4179–4192.
3 T. Famprikis, P. Canepa, J. A. Dawson, M. S. Islam and C. Masquelier, *Nat. Mater.*, 2019, **18**, 1278–1291.
4 K. J. Kim, M. Balaish, M. Wadaguchi, L. Kong and J. L. M. Rupp, *Adv. Energy Mater.*, 2021, **11**, 2002689.
5 C. Li, S. Zhang, X. Miao, C. Wang, C. Wang, Z. Zhang, R. Wang and L. Yin, *Batteries Supercaps*, 2022, **5**, e202100288.
6 R. Kanno, *Electrochemistry*, 2023, **91**, 102001.
7 L. Jia, J. Zhu, X. Zhang, B. Guo, Y. Du and X. Zhuang, *Electrochem. Energy Rev.*, 2024, **7**, 12.
8 X. Zhang, S. Cheng, C. Fu, G. Yin, L. Wang, Y. Wu and H. Huo, *Nano-Micro Lett.*, 2025, **17**, 2.
9 T. Yu, Y. Liu, H. Li, Y. Sun, S. Guo and H. Zhou, *Chem. Rev.*, 2025, **125**, 3595–3662.
10 G. Oh, M. Hirayama, O. Kwon, K. Suzuki and R. Kanno, *Chem. Mater.*, 2016, **28**, 2634–2640.
11 Y. Morino and S. Kanada, *J. Power Sources*, 2021, **509**, 230376.
12 R. Koerver, I. Aygün, T. Leichtweiß, C. Dietrich, W. Zhang, J. O. Binder, P. Hartmann, W. G. Zeier and J. Janek, *Chem. Mater.*, 2017, **29**, 5574–5582.
13 J.-M. Doux, H. Nguyen, D. H. S. Tan, A. Banerjee, X. Wang, E. A. Wu, C. Jo, H. Yang and Y. S. Meng, *Adv. Energy Mater.*, 2020, **10**, 1903253.
14 K. Watanabe, H. Nakayama, H.-S. Kim, K. Hikima, N. Matsui, K. Suzuki, S. Obokata, H. Muto, A. Matsuda, R. Kanno and M. Hirayama, *Electrochemistry*, 2025, **93**, 063019.
15 K. Watanabe, H.-S. Kim, K. Hikima, N. Matsui, K. Suzuki, H. Muto, A. Matsuda, R. Kanno and M. Hirayama, *Batteries Supercaps*, 2025, **8**, e202500119.
16 N. Ohta, K. Takada, I. Sakaguchi, L. Zhang, R. Ma, K. Fukuda, M. Osada and T. Sasaki, *Electrochem. Commun.*, 2007, **9**, 1486–1490.
17 N. Ohta, K. Takada, L. Zhang, R. Ma, M. Osada and T. Sasaki, *Adv. Mater.*, 2006, **18**, 2226–2229.
18 J. S. Du, Y. Bae and J. J. De Yoreo, *Nat. Rev. Mater.*, 2024, **9**, 229–248.
19 J. Mu, S. Liao, L. Shi, B. Su, F. Xu, Z. Guo, H. Li and F. Wei, *Polym. Chem.*, 2024, **15**, 473–499.
20 S. Duan, L. Qian, Y. Zheng, Y. Zhu, X. Liu, L. Dong, W. Yan and J. Zhang, *Adv. Mater.*, 2024, **36**, 2314120.

21 H. Kim, M. G. Kim, H. Y. Jeong, H. Nam and J. Cho, *Nano Lett.*, 2015, **15**, 2111–2119.
22 G.-L. Xu, Q. Liu, K. K. S. Lau, Y. Liu, X. Liu, H. Gao, X. Zhou, M. Zhuang, Y. Ren, J. Li, M. Shao, M. Ouyang, F. Pan, Z. Chen, K. Amine and G. Chen, *Nat. Energy*, 2019, **4**, 484–494.
23 Q. Gan, N. Qin, Y. Zhu, Z. Huang, F. Zhang, S. Gu, J. Xie, K. Zhang, L. Lu and Z. Lu, *ACS Appl. Mater. Interfaces*, 2019, **11**, 12594–12604.
24 G. Hu, J. Fan, Y. Lu, Y. Zhang, K. Du, Z. Peng, L. Li, B. Zhang, Y. Shi and Y. Cao, *ChemSusChem*, 2020, **13**, 5699–5710.
25 S. Tubtimkuna, D. L. Danilov, M. Sawangphruk and P. H. L. Notten, *Small Methods*, 2023, **7**, 2300345.
26 C. Huang, C. L. A. Leung, P. Leung and P. S. Grant, *Adv. Energy Mater.*, 2021, **11**, 2002387.
27 M. Ihrig, E. Dashjav, A. M. Laptev, R. Ye, D. Grüner, M. Ziegner, P. Odenwald, M. Finsterbusch, F. Tietz, D. Fattakhova-Rohlfing and O. Guillon, *J. Power Sources*, 2022, **543**, 231822.
28 M. C. Nguyen, H. L. Nguyen, T. P. M. Duong, S.-H. Kim, J.-Y. Kim, J.-H. Bae, H.-K. Kim, S. N. Lim and W. Ahn, *Adv. Funct. Mater.*, 2024, **34**, 2406987.
29 J. Yu, Y. Wang, L. Shen, J. Liu, Z. Wang, S. Xu, H. M. Law and F. Ciucci, *Adv. Mater.*, 2025, **37**, 2417796.
30 S. Z. Zhang, X. H. Xia, D. Xie, R. C. Xu, Y. J. Xu, Y. Xia, J. B. Wu, Z. J. Yao, X. L. Wang and J. P. Tu, *J. Power Sources*, 2019, **409**, 31–37.
31 R. Amin, U. Nisar, M. M. Rahman, M. Dixit, A. Abouimrane and I. Belharouak, *J. Mater. Chem. A*, 2024, **12**, 14186–14205.
32 L. Porcarelli, A. S. Shaplov, M. Salsamendi, J. R. Nair, Y. S. Vygodskii, D. Mecerreyes and C. Gerbaldi, *ACS Appl. Mater. Interfaces*, 2016, **8**, 10350–10359.
33 J. L. Olmedo-Martínez, L. Porcarelli, Á. Alegría, D. Mecerreyes and A. J. Müller, *Macromolecules*, 2020, **53**, 4442–4453.
34 L. Porcarelli, P. Sutton, V. Bocharova, R. H. Aguirresarobe, H. Zhu, N. Goujon, J. R. Leiza, A. Sokolov, M. Forsyth and D. Mecerreyes, *ACS Appl. Mater. Interfaces*, 2021, **13**, 54354–54362.
35 S. Sen, E. Trevisanello, E. Niemöller, B.-X. Shi, F. J. Simon and F. H. Richter, *J. Mater. Chem. A*, 2021, **9**, 18701–18732.
36 S. W. Thompson, T. R. Guimarães, K. Watanabe, M. Hirayama and P. B. Zetterlund, *Polymer*, 2025, **324**, 128255.
37 E. Bourgeat-Lami, F. D'Agosto and M. Lansalot, in *Controlled Radical Polymerization at and from Solid Surfaces*, ed. P. Vana, Springer International Publishing, Cham, 2016, vol. 270, pp. 123–161.
38 G. Moad, E. Rizzardo and S. H. Thang, *Aust. J. Chem.*, 2012, **65**, 985–1076.
39 D. Nguyen, H. S. Zondanos, J. M. Farrugia, A. K. Serelis, C. H. Such and B. S. Hawkett, *Langmuir*, 2008, **24**, 2140–2150.
40 E. Bourgeat-Lami, A. J. P. G. França, T. C. Chaparro, R. D. Silva, P.-Y. Dugas, G. M. Alves and A. M. Santos, *Macromolecules*, 2016, **49**, 4431–4440.
41 T. R. Guimarães, M. Lansalot and E. Bourgeat-Lami, *J. Mater. Chem. B*, 2020, **8**, 4917–4929.
42 D. Nguyen, C. H. Such and B. S. Hawkett, *J. Polym. Sci., Part A: Polym. Chem.*, 2013, **51**, 250–257.
43 V. T. Huynh, D. Nguyen, C. H. Such and B. S. Hawkett, *J. Polym. Sci., Part A: Polym. Chem.*, 2015, **53**, 1413–1421.
44 A. C. Perreira, S. Pearson, D. Kostadinova, F. Leroux, F. D'Agosto, M. Lansalot, E. Bourgeat-Lami and V. Prévot, *Polym. Chem.*, 2017, **8**, 1233–1243.
45 T. C. Chaparro, R. D. Silva, P.-Y. Dugas, F. D'Agosto, M. Lansalot, A. M. dos Santos and E. Bourgeat-Lami, *Polym. Chem.*, 2021, **12**, 69–81.
46 W. Peng, Y. Cai, L. Fanslau and P. Vana, *Polym. Chem.*, 2021, **12**, 6198–6229.
47 P. Sarkar, S. Ghosh, R. Saha and K. Sarkar, *RSC Adv.*, 2021, **11**, 16913–16923.
48 W. J. Li, M. Hirayama, K. Suzuki and R. Kanno, *Solid State Ionics*, 2016, **285**, 136–142.
49 T. Yabuzaki, M. Sato, H. Kim, K. Watanabe, N. Matsui, K. Suzuki, S. Hori, K. Hikima, S. Obokata, H. Muto, A. Matsuda, R. Kanno and M. Hirayama, *J. Ceram. Soc. Jpn.*, 2023, **131**, 675–684.
50 H.-S. Kim, K. Watanabe, N. Matsui, K. Suzuki, R. Kanno and M. Hirayama, *Batteries Supercaps*, 2023, **6**, e202300306.
51 Y. Yamada, K. Watanabe, H.-S. Kim, K. Suzuki, S. Hori, R. Kanno and M. Hirayama, *Batteries Supercaps*, 2023, **6**, e202300261.
52 T. Ohzuku and A. Ueda, *J. Electrochem. Soc.*, 1994, **141**, 2972.